Evolution of electronic structure on Transition Metal doped Titanium Disulfide by angle-resolved photoemission spectroscopy study

X. Y. Cui,[1,*] H. Negishi,[2] A. N. Titov,[3] S. G. Titova,[4] M. Shi,[1] and L. Patthey[1]

[1]*Swiss Light Source, Paul Scherrer Institute, CH-5232 Villigen, Switzerland*
[2]*Department of Materials Sciences, Faculty of Science, Hiroshima University, Higashi Hiroshima 739-8526, Japan*
[3]*Institute of Metal Physics, Urals Division of RAS, 620219 Yekaterinburg GSP-170, Russia*
[4]*Institute of Metallurgy, Urals Division of RAS, 620016 Yekaterinburg, Russia*

(Dated: October 19, 2021)

We have systematically investigated the structural property and electrical structures of the transition metal intercalated titanium disulfide compound Fe_xTiS_2 ($0 \leq x \leq 0.33$) from angle-resolved photoelectron spectroscopy with tunable polarized synchrotron radiation. The effect of intercalation on the energy bands and density of states of the host material around two high-symmetry points (Γ, L) is studied. Charge transfer from the Fe atoms to the dichalcogenide layers leads to the movement of the Ti 3d-derived electron pocket. Two hybridized states are observed around ~ 500 meV and Fermi level. Knowledge of hybridization among the Fe 3*d*, Ti 3*d*, and S 3*p* states is very important to understand the physical of Fe_xTiS_2 system.

PACS numbers: 71.20.-b, 71.45.Lr, 79.60.-i

I. INTRODUCTION

Recently, transition-metal dichalcogenides (TMDC) provide an important playground of interesting physics. The type and concentration of the intercalated guest atoms entering into Van der Waals gaps of titanium dichalcogenide will dramatically effect the physical properties and electronic structure of the host material. No surprise that from the very beginning several issues have been hotly debated in the field: the modification of the electronic structure and the origin of this modification. As a good example, intercalation of transition metals in titanium dichalcogenides' van der Waals gap (as shown in Fig. 1(a)) often leads to the formation of narrow and non-dispersive bands close to the Fermi level in contrary with intercalation of alkali metals where the rigid band model is successfully applied.[1–10]

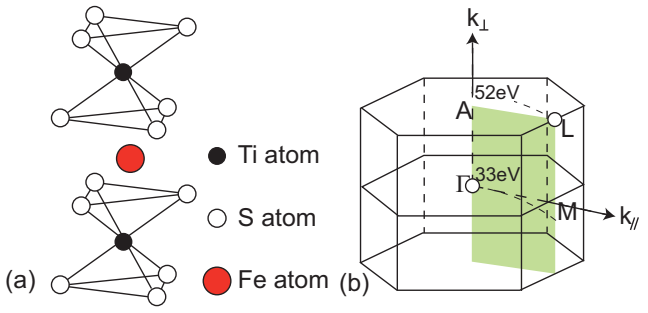

FIG. 1: (a) Coordination of the Ti, Fe and S atoms in 1T structure, (b)First Brillouin zone (BZ) of 1T-TiS_2 and contours in k plane at E_F by scanning polar angle $\theta \leq 25$ ° in the ARPES experiment for hν=33 and 52 eV.

These non-dispersive bands describe localized character of electronic states without Fermi level crossing. It is due to the successive formation of covalent complex bonds between intercalant and its nearest lattice surrounding. This complex plays a trapping role for conducting electrons. This is a result of competition between lattice strain and covalent interactions of intercalant ion and host lattice. Lattice expansion caused by insertion of guest atoms while covalent interaction results in lattice compression in normal direction to basal plane and formation of flat band below Fermi level. For M_xTiTe_2 system, band structure calculation shown that these new formed bands are the result of hybridization between 3d-states of intercalant and surrounding $TiTe_2$ lattice, mainly Ti $3d_{z^2}$ states.[1] Experimental Angle-resolved photoemission spectroscopy (ARPES) measurements for Fe_xTiTe_2 and Fe_xTiSe_2[5,6] also shown the presence of hybridized bands with binding energy ~ 0.3 eV below Fermi level. In this case, the comprehensive understanding of concentration effect in Fe_xTiS_2 system serves as a good starting point towards ultimate view of the physics of the coupling of these hybridized band, valence band and electron pocket at different intercalation.

In present work we used High-resolution ARPES as powerful tool to study the electronic structure of Fe_xTiS_2 system with two aims: 1. to have the fundamental knowledge of the band structure of non-doped TiS_2; 2. to establish the modification of band structure due to the intercalation of iron in TiS_2 and the mechanism of the formation of these localized states.

II. EXPERIMENTAL RESULTS

Fe_xTiS_2 ($0 \leq x \leq 0.33$) were grown by a chemical vapor transport technique in a single-zone furnace with a small temperature gradient. Fe_xTiS_2 were grown in the form of thin flakes up to 8 x 8 mm^2 with thickness 0.05-1 mm. All the grown crystals were shown by X-

ray diffraction to have a 1T-CdI_2 type structure over the whole composition range $0 \leq x \leq 1$. The values of the lattice constants of single-crystals as a function of the Fe concentration are in a good accordance with literature data[8], which confirms the Fe concentration obtained from the x-ray microanalyzer.

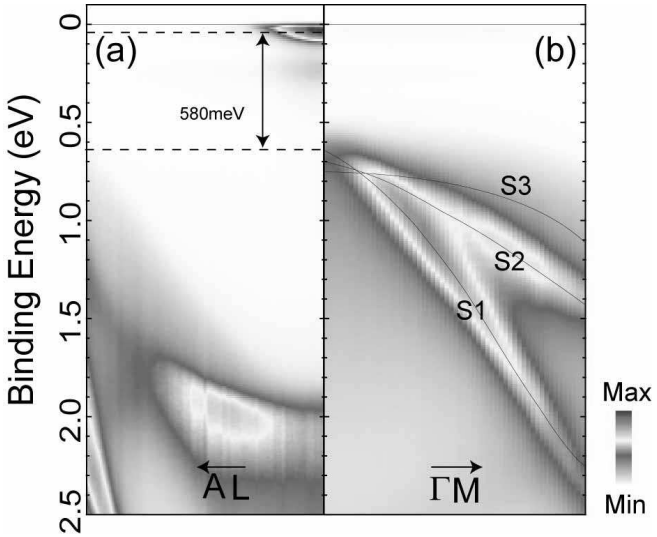

FIG. 2: Photoemission intensity plots for TiS_2 were compared at L (for hν=52 eV) (a) and Γ (for hν=33 eV) (b) points at 10 K. S1, S2 and S3 lines in (b) are the dispersions of three S 3p-derived bands, obtained from band structure calculation[13]. Dashed lines in (a) correspond to the energies of the bottom of the Ti-3d derived spectral feature and the top of the S1 band. Arrows in (a) illustrate the distance between the valence band and the spectral feature.

Our samples were cleaved and measured in an ultra-high vacuum preparation chamber with a pressure below 1×10^{-11} mbar. The crystal orientation was determined by the low-energy electron diffraction (LEED). The cleanliness of the surface was checked by X-ray photoelectron spectroscopy (XPS) just before and after the ARPES measurement. During the measurement, the sample was mounted on a low-temperature goniometer with a six-degree of freedom manipulator (CARVING) and cooled down below 10 K. The ARPES measurements were performed with Circular polarization at the Surface and Interface Spectroscopy (SIS) Beamline[11] at the Swiss Light Source (SLS), Paul Scherrer Institute (PSI). The multi-channel angular mode of the hemispherical electron-energy analyzer (R4000 SCIENTA) was used for high-resolution ARPES measurements. Total-energy resolution was set at 10 meV to get a sufficient intensity. Angular resolution was better than $\Delta\theta$=0.1 ° (Δk=0.01 $Å^{-1}$). The Fermi level was determined by recording the photoemission spectrum from polycrystalline copper on the sample holder.

The light was incident onto the sample surface at 45 ° relevant to the analyzer axis. The sample was rotated in the horizontal plane including the Γ(A)-M(L) axis for the polar angle scanning as Fig. 1(b). The parallel and perpendicular components of the photoelectron wave vectors relative to the sample surface, $k_{\|}$ and $k_{\perp}$, were determined in the free-electron approximation by the equations $k_{\|} = \sqrt{2mE_k/\hbar^2}sin\theta$ and $k_{\perp} = \sqrt{2m(E_k cos^2\theta + V_0)/\hbar^2}$, where E_k is the kinetic energy of the photoelectron, V_0 is the inner potential[12]. Here we assumed V_0 = 11 eV by considering the symmetry of the experimentally derived band structure near the high symmetry point and on the basis of the results obtained by previous measurement[9]. The photon energy (hν) was selected between 25-55 eV, according to the arcs in Fig. 1(b).

Firstly, we focus on the detailed band structure of undoped TiS_2. Figures 2(a) and 2(b) show the intensity plots at L point and Γ point. A spectral feature at binding energy ($E_B \sim$ 30 meV) is observed at the L point in 2(a), showing the existence of a Ti 3d-derived pocket around the Fermi level (E_F), in agreement with previous band-structure calculation[13,16]. The bottom of this feature is $\sim 40 \pm 5$ meV. S1, S2 and S3 solid lines in 2(b) are the dispersions of three S 3p-derived bands from the LDA calculation[13,16]. The maxima of S 3p-derived valence bands at the Γ point are $E_B \sim$ 620 meV (S1), 700 meV (S2) and 750 meV (S3), respectively. Our data did not reveal the presence of hole at Γ point, predicted as a semimetal or metal by other band structure calculations.[14] There is a gap as large as 580 meV between the S 3*p*-derived valence band S1 and Ti 3*d*-derived pocket, whose positions are well defined by the centroid of the spectra. Generally, our TiS_2 data are taken as evidence for the semiconductor character. Since the electronegativity of the S atom is 2.5 which is smaller than Se, it is expected that the valence bands in TiS_2 should be deeper than in $TiSe_2$ ($\sim$ 160 meV in previous reports[6,10]), and the p-d indirect band overlap in TiS_2 density of states would be smaller or even nonexistent. In the meantime, one state with weak intensity appears around $E_B \sim$ 220 meV at L (Fig. 2(a)) and Γ (Fig. 2(b)) points (it is even clearer from the energy distribution curve (EDC) in Figures. 3, 4 and 5). The appearance is probably related to the non-stoichiometry of the crystals. Brauer et al., also suggested, in practice, there is always excess Ti present, leading to partial filling of the Ti 3d-derived conduction band.[15,16]

Furthermore, some measurements by Thompson suggested the existence of the superlattice and subtle plateau, which is close to the distortion temperature predicted with CDW state in the layered dichalcogenides[17,18]. In CDW phase, a $2a\times2a\times2c$ superlattice forms and the valence bands at Γ point is folded to L region. There is no evidence to prove this CDW phase transition from our LEED and ARPES measurements for all the samples at different temperatures.

Figures 3(a, b, c, and d) are the second derivative of the photoemission intensity along the energy direction. (in a linear terrain scale; the blue portion indicates the

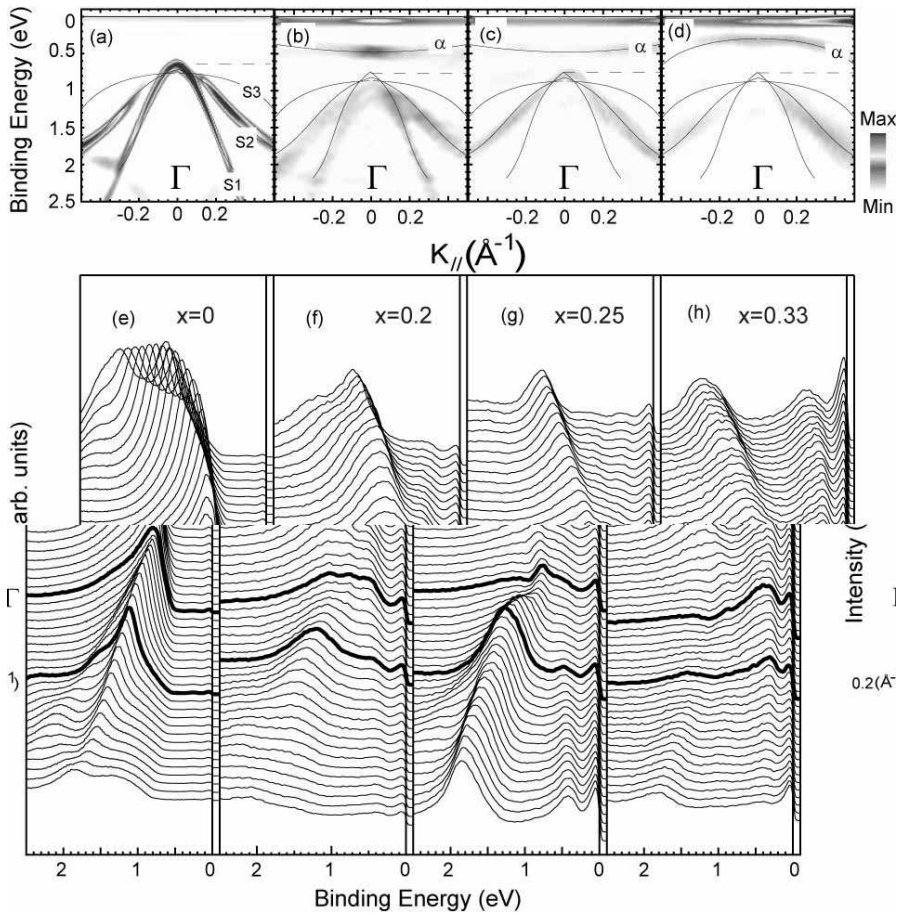

FIG. 3: The second derivative of the photoemission intensity along the energy direction(a, b, c, d) (for better contrast of the measured band structures) and EDCs (e, f, g, h) for Fe_xTiS_2 (x=0, 0.2, 0.25, 0.33) at Γ point through Γ-M direction for hν=33 eV at 10 K. S1, S2 and S3 lines in (a) are the dispersions of three S 3p derived bands, obtained from MDC analysis. α band in (b, c, d) is Fe hybridized structure. Thick lines in (e, f, g, h) correspond to the EDCs at Γ and $k_{\|} = 0.2\AA$ points for different doping.

highest spectral intensity, that is, where the energy bands are located) and energy distribution curves(EDCs) at Γ point through Γ-M direction on Fe_xTiS_2 (x=0, 0.2, 0.25, 0.33) samples measured at $h\nu$ = 33 eV at 10 K, respectively. With increased Fe concentration, One new state starts to develop around 500 meV in Figures 3(b, c, and d). A bond formation between Fe $3d_{z^2}$ and Ti $3d_{z^2}$ states should be responsible for this new band, taking into account that similar structure also appear in Fe_xTiSe_2 and Fe_xTiTe_2[5,6]. The character of covalent bonding is much weaker in the Fe-S bond than in the Fe-Se and Fe-Te ones because the electronegativity of the S atom is 2.5 which is larger than that of Se and Te atoms. The maxima of S1, S2 and S3 valence bands shifts from 620, 700 and 750 meV to 780, 830 and 880 meV as a function of x.

With the movement of S valence bands, the curvature of α band attains amaximum at x = 0.2 and vanishes for x=0.25 and 0.33.

This behavior may coincide with the change of the lattice constants a, c, as listed in Table 1.

TABLE I: A list of parameters of Fe_xTiS_2 (x= 0, 0.2, 0.25 and 0.33)

x	0	0.2	0.25	0.33
a($\AA$)	3.412	3.413	3.416	3.420
c($\AA$)	5.722	5.716	5.718	5.720
$S1_{max}$(meV)	620	780	780	780
$S3_{max}$(meV)	750	880	880	880
α_{center}(meV)	–	490	490	300
L_{min}(meV)	40	99	110	140

In order to understand the nature of the new hybridized band α, we should pay attention to the modification of lattice constants due to Fe doping. From related X-ray powder diffraction (XRD) experiment, the lattice parameter a increases from 3.412 to 3.420 Å with x=0 to 0.33; and c axis slightly decreases from 5.722 Å (x=0) to 5.720 Å (x=0.33)[8]. This modification in parameter c and a clearly suggests that the guest iron atoms intercalate into the van der Waals gap of the TiS_2, but don't

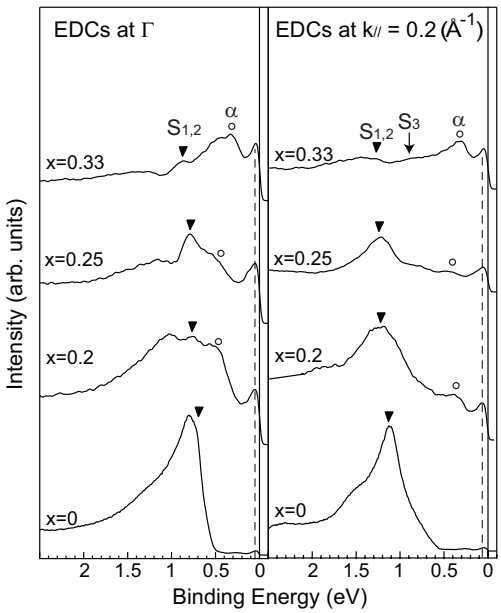

FIG. 4: EDCs at 0 (Γ point) and $k_{\|}$=0.2 $\AA$ for Fe_xTiS_2 (x=0, 0.2, 0.25, 0.33) around Γ point for hν=33 eV at 10 K. Inverse triangle and inverse arrow correspond to the maximum of S1 and S2 bands and the maximum of S3 band. Open circle, tick-mark and open square correspond to the location of α, β, γ bands.

substitute Ti atoms. Such a variation is also strongly suggestive of a weak destruction of the periodicity along the c axis due to a random bridging of the layers between the intercalated Fe atoms with Ti-Fe-Ti chains. Previous results of Fe Mössbauer spectra observed the values of isomer shift are 0.7-0.8 mm/s for all the Fe doped TiS_2,[8] which corresponds to the existence of new compound (FeS) where the iron atoms are surrounded octahedrally by S atoms and the Fe-S bond is rather covalent, indicating that the Fe atom starts to occupy the octahedral site in the gap and becomes the divalent ion Fe^{2+} with higher spin state.

Fig. 4 show the EDCs at Γ and $k_{\|}$=0.2 $\AA$ for x=(0, 0.2, 0.25, 0.33), Inverse triangle and inverse arrow correspond to the maximum of S1 and S2 bands and the maximum of S3 band. Open circle, tick-mark and open square correspond to the location of α, β, γ bands. S1, S2, β bands shift towards high energy direction; S3 and α bands shift towards E_F; γ band has negligible movement with increased x. Because α band is closer to S3 than S1 and S2, which make S3 strongly couple with the closest α band and move towards E_F. Then S1, S2 bands move to the opposite direction caused by Fe scattering potential. From Table.1, the evolution of S1, S2 and α bands are still be explained by rigid-band model; others cannot. It is noted that the locations of new α, β, γ structures are different with the result of other Fe doped TMDC system. In previous ARPES experiments, appearance of hybridized bands was observed at E_F and 0.3 eV in Fe_xTiSe_2 and Fe_xTiTe_2 and explained as a result of Ti-Fe-Ti bonding.[5,6] The reason is the difference in the degree of filling of Ti $3d_{z^2}$ - states is high enough in $TiSe_2$ materials. But in TiS_2, these states are empty (Fig. 2) so formation of these bands is mainly caused by hybridization of S3p/Fe3d_{z^2} - states. As it was shown in ref. [1] and [6], states of chalcogen are always mixed with hybrid M3d_{z^2}/Ti3d_{z^2} band. For TiS_2, empty Ti 3d-states and S 3p-states provide main contribution in $\beta and \gamma$ hybrid states in particular, it manifests through lattice compression in direction normal to the basal plane.

Meanwhile, in Fig.4, the EDCs show enhanced density of state close to E_F for x=0.2 to 0.33. This is shown by the thin line at E_B approx. 100 meV. As described above, this contribution is mainly associated to the overdoped Ti atoms. there contains strong density of states at E_F. Another possibility is the lowest conduction band shifting down into a lower position, due to the iron intercalation substantially modifies both the lattice and electronic structures of TiS_2 material. Some tight-binding linear muffin-tin orbital (TB-LMTO) band-structure calculation suggests the direct gap between conduction band and valence band at Γ of TiS_2 is around 150 meV[13], which is roughly close to our measurement. But from angle-resolved inverse photoemission spectroscopy (IPES) experiment[20], the closest conduction band at Γ point is around 1 eV above the E_F. Due to the limited IPES energy resolution, one must pay attention to this effect.

Figures 5(a,e), (b,f), (c,g), (d,h) show the intensity plots and MDCs at L point through A-L direction on Fe_xTiS_2 (x=0, 0.2, 0.25, 0.33) samples measured at hν=52 eV at 10 K, respectively. A spectral feature is observable at the L point as a function of x. The black dotted line close to E_F in Figures 5(a, b, c, d) is the dispersion of Ti 3d-derived electronic pocket, obtained from EDC analysis. The bottom of electronic pocket shifts from $E_B \sim 40$ meV to 150meV with x. Thick line in Figures 5(e, f, g, h) corresponds to the MDCs at E_F with x. These MDCs can be fit with two Lorentzians, which confirms the electron pocket character of this spectral feature. With increasing x, this electron pocket shifts toward high binding energy and increases in intensity reflecting the enhancement of the metallic character of TiS_2 by Fe concentration.

Dashed line around $E_B \sim 550$ meV in Figures 5(b, c, d) corresponds to the modification of the hybridized band obtained from EDC analysis. This band shows negligible dispersion in Fig. 5(b) (x=0.2) and notable dispersion within 200 meV in Fig. 5(d) (x=0.33). This feature underlines that this band is originated from a localized state rather than a band-like state. For large x, this dispersion starts to develop, together with the coupling with the neighbor electron pocket. We introduce the coupling model below to explain this development. In the meantime, we should mention that the strong intensity from the electron pocket does not allow us to determine the development of the tiny impurity band (due to Ti over-

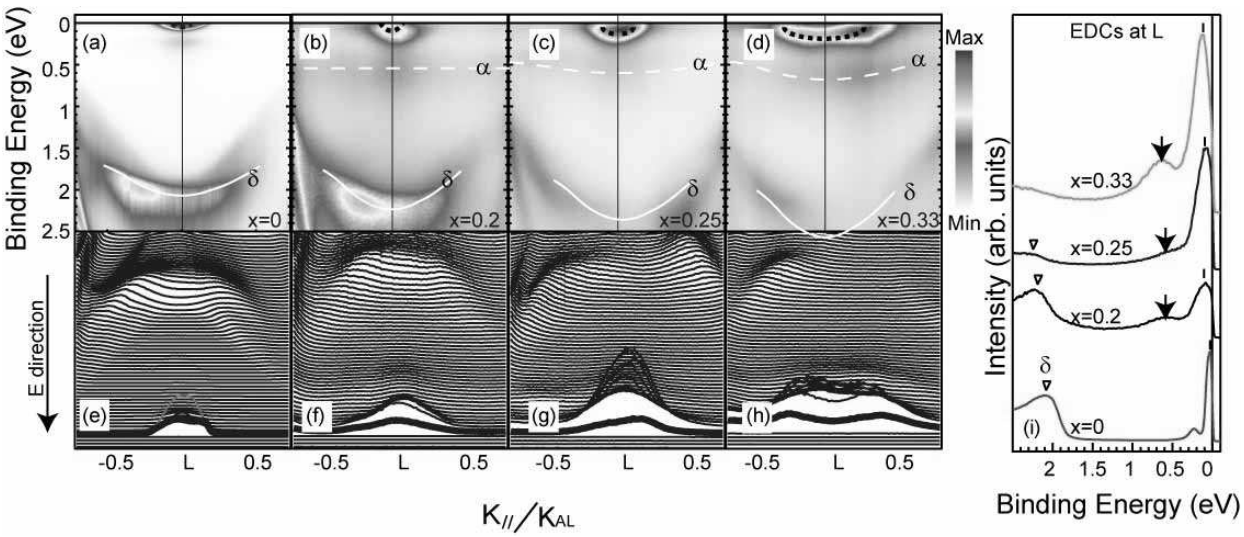

FIG. 5: The intensity plots (a, b, c, d) and MDCs (e, f, g, h) for Fe_xTiS_2 (x=0, 0.2, 0.25, 0.33) at L point through A-L direction for hν=52 eV at 10 K. (i) EDCs at L point for Fe_xTiS_2 (x= 0, 0.2, 0.25, 0.33) for hν= 52 eV at 10K. Thick dotted line close to E_F in (a, b, c, d) is the dispersion of Ti 3d-derived pocket, obtained from MDC analysis. Dashed line around $E_B \sim 550$ meV in (b, c, d) corresponds to the dispersions of the Ti-Fe 3d-3d hybridized band, obtained from EDC analysis. Solid line between $E_B \sim 1.5-2$ eV in (a, b, c) corresponds to the dispersion of the S $3p_\sigma$ derived band. The inverse empty triangle in (i) notes the location of S $3p_\sigma$ derived state at L point. Arrow and dashed line in (i) correspond to the locations of the hybridized band at L point. Thin line at low E_B in (i) corresponds to the location of the minimum of the electron pocket at L point. Thick line in (e, f, g, h) corresponds to the MDC at E_F for different doping.

doping at $E_B \sim 0.25$ eV). This will not influence our physical discussion.

Band structure calculation[9] suggests the half of S $3p_\sigma$-derived state forms the state at $E_B \sim 2$ eV in Figures 5(a, b, c)(white line) and Fig. 5(i). This state strongly modified by Fe doping, shifts to larger E_B from x=0 to 0.25, then moves away from the energy window at x=0.33. This movement is barely observed for Ni intercalated TiS_2[9].

From previous experimental data[8,9] on M_xTiS_2 (M=Fe, Ni), it is known that Fe atom becomes the divalent ion Fe^{2+}, as well as Ni atom becomes Ni^{2+}. The difference between them is the potential of ionization: 16,188 eV for Fe^{2+} and 18,169 eV for Ni^{2+}. This leads to the appearance of the impurity states at higher binding energy for Ni_xTiS_2 in comparison with Fe_xTiS_2 and, as a consequence, to higher localization degree for electrons in the impurity band of Ni_xTiS_2 in comparison with Fe_xTiS_2.

Fig. 5(i) shows the EDCs at L point for x=(0, 0.2, 0.25, 0.33). The maximum of state at larger binding energy (inverse empty triangle at $E_B \sim 2$ eV) moves away from E_F as a function of x. The tick-mark at low energy location slightly moves away from E_F also, coincided with the bottom of occupied electron pocket. The notable change is the shift of the hybridized band (dashed line around high E_B(~ 0.5 eV), which will be explained below.

III. DISCUSSION

To clarify the development of these structures, we construct a coupling model. This coupling model is based on the possible band mixing between S valence bands, Fe-Ti hybridized bands and electron pocket. When Fe intercalation starts, the flat localized state (B_α) forms around $E_B \sim 500$ meV in Figures 6(c, d); with increased Fe content, the Ti 3d band (electron pocket) (B_e) becomes more occupied and shifts away from E_F, and the corresponding B_α starts to slightly bend itself down, as shown in Fig. 6(d). When the bottom of B_e starts to energetically coupled with B_α, the center of B_e shifts towards E_F and the curvature of B_α is enhanced to larger binding energy, which correspond to the modification of these two bands in the intensity plots in Fig. 5(d). An additional important point is B_α's bending magnitude is ~ 100 meV for x=0.33, which coincides with the shift of the hybridized band at L point in 5(d). We would like to point out that our preliminary calculations confirmed the existence of these hybridized structures. At the very least we were still not able to fully clarify β and γ structures. The continuous calculation is needed in the future.

J. Rasch et al. used H_2O adsorption onto the van der Waals-like surface between Titanium dichalcogenides layers,[22] causing a distinct bending of the bands and resulting in a filled lowest conduction band. By looking at filled Ti conduction band, the indirect gap can be detected. This would be another idea to verify the detailed movement of our band structure and confirm our previ-

ous and recent conclusion on Titanium dichalcogenides system, associated with high-resolution ARPES experiment.

Meantime, the long list of analogies of recent layered TMDC (resistivity and doping) can now explain the competition between CDW and superconductivity. Superconductivity with critical temperature around 14K was reported in the Fe-Se-Te compound[23]. This discovery also needs a fresh angle to the fundamental physics of the d-p coupling between Fe-S, Fe-Se and Fe-Te compounds. Our work will be critical to understand the unconventional properties in this system.

IV. SUMMARY

To summarize, using high-resolution ARPES, TiS_2 is proved to be a semiconductor. We confirmed that there is no CDW transition happen. Upon iron guest atoms intercalation, the strong modification of the valence bands and electron pocket in the intercalated compound Fe_xTiS_2 are revealed. The hybridization of the Ti 3d-derived states with the Fe 3d states is thought to be predominantly the reason. The coupling model has been introduced to explain the mechanism of modification of these hybridized bands.

V. ACKNOWLEDGMENTS

The measurements were done at Surface and Interface Spectroscopy (SIS) Beamline, Swiss Light Source, Paul Scherrer Institute, Villigen, Switzerland. We thank C. Hess and F. Dubi for technical support. We also thank V. N. Strocov, C. Monney for helpful discussion on the mechanism of transition metals doping and useful comments.

* xiaoyu.cui@psi.ch

[1] T. V. Kuznetsova, A. N. Titov, Yu. M. Yarmoshenko, E. Z. Kurmaev, A. V. Postnikov, V. G. Pleschev, B. Eltner, G. Nicolay, D. Ehm, S. Schmidt, F. Reinert, and S. Hüfner, Phys. Rev. B. **72**, 085418 (2005).

[2] H. Cercellier, C. Monney, F. Clerc, C. Battaglia, L. Despont, M. G. Garnier, H. Beck, P. Aebi, L. Patthey, H. Berger and L. Forró, Phys. Rev. Lett. **99**, 146403 (2007).

[3] A. N. Titov, A. V. Kuranov, V. G. Pleschev, Yu. M. Yarmoshenko, M. V. Yablonskikh, A. V. Postnikov, S. Plogmann, M. Neumann, A. V. Ezhov and E. Z. Kurmaev, Phys. Rev. B **63**, 035106 (2001).

[4] A. N. Titov, Yu. M. Yarmoshenko, A. Zimina, M. V. Yablonskikh, A. V. Postnikov and S. Eisebitt, Physics of the Solid State **50**, 1186 (2008).

[5] K. Yamazaki, K. Shimada, H. Negishi, F. Xu, A. Ino, M. Higashiguchi, H. Namatame, M. Taniguchi, M. Sasaki, S. Titova, A. Titov and Yu. M. Yarmoshenko, Physica B: Condenced Matter **351** 262 (2004).

[6] X. Y. Cui, H. Negishi, S. G. Titova, K. Shimada, A. Ohnishi, M. Higashiguchi, Y. Miura, S. Hino, A. M. Jahir, A. Titov, H. Bidadi, S. Negishi, H. Namatame, M. Taniguchi, and M. Sasaki, Phys. Rev. B **73**, 085111 (2006).

[7] S. G. Titova, A. N. Titov, Physics of the Solid State **49**, 63 (2007).

[8] M. Inoue, Y. Muneta, H. Negishi, and M. Sasaki, J. Magn. Magn. Mater. **53**, 131 (1985).

[9] T. Matshushita, S. Suga, and A. Kimura, H. Negishi, M. Inoue, Phys. Rev. B **60**, 1678 (1999).

[10] J. F. Zhao, H. W. Ou, G. Wu, B. P. Xie, Y. Zhang, D. W. Shen, J. Wei, L. X. Yang, J. K. Dong, M. Arita, H. Namatame, M. Taniguchi, X. H. Chen, and D. L. Feng, Phys. Rev. Lett. **99**, 146401 (2007).

[11] X. Y. Cui, E. E. Krasovskii, V. N. Strocov, A. Hofmann, J. Schäfer, R. Claessen, and L. Patthey, Phys. Rev. B **81**, 245118 (2010).

[12] S. Hüfner, *Photoelectron Spectroscopy (3rd Ed.)*, Springer-Verlag, 2003.

[13] Z. Y. Wu, F. Lemoigno, P. Gressier, G. Ouvrard, P. Moreau, and J. Rouxel, C. R. Natoli, Phys. Rev. B **54**, R11009 (1996).

[14] C. M. Fang, R. A. de Groot, and C. Haas, Phys. Rev. B **56**, 4455 (1997).

[15] R. Claessen, R. O. Anderson, G.-H. Gweon, and J. W. Allen, W. P. Ellis, C. Janowitz, C. G. Olson, Z. X. Shen, V. Eyert, M. Skibowski, K. Friemelt, E. Bucher, and S. Hüfner, Phys. Rev. B **54**, 2453 (1996).

[16] H. E. Brauer, H. I. Starnberg, L. J. Holleboom, H. P. Hughes and V. N. Strocov, J. Phys.: Condens. Matter **11**, 8957 (1999).

[17] A. H. Thompson, Phys. Rev. Lett. **34**, 520 (1975); A. H. Thompson, Phys. Rev. Lett. **35**, 1786 (1975).

[18] C. H. Chen, W. Fabian, F. C. Brown, K. C. Woo, B. Davies, and B. DeLong, A. H. Thompson, Phys. Rev. B **21**, 615 (1980).

[19] A. Zunger, A. J. Freeman, Phys. Rev. B **16**, 906 (1979).

[20] S. Nohara, H. Namatame, H. Matsubara, M. Fujisawa, M. Naitou, S. Tanaka, H. Negishi, M. Inoue, H. Sakamoto, A. Misu, and S. Suga, J. Phys. Soc. Jap. **60**, 3882 (1991).

[21] H. Martinez, Y. Tison, I. Baraille, M. Loudet, D. Gonbeau, J. Electron Spectrosc. Relat. Phenom. **125**, 181 (2002).

[22] Julia C. E. Rasch, Torsten Stemmler, Beate Müller, Lenart Dudy, and Recardo Manzke, Phys. Rev. Lett. **101**, 237602 (2008).

[23] F.-C. Hsu et al., PNAS **105**, 14262 (2008).